MOLECULAR AND CELLULAR BIOLOGY, July 2009, p. 3915–3928 Vol. 29, No. 14
0270-7306/09/$08.00+0 doi:10.1128/MCB.01199-08

NADPH Oxidase 1 Controls the Persistence of Directed Cell Migration by a Rho-Dependent Switch of α2/α3 Integrins▽†

Amine Sadok,[1] Anne Pierres,[2] Laetitia Dahan,[1] Charles Prévôt,[1] Maxime Lehmann,[1] and Hervé Kovacic[1]*

INSERM UMR 911, CRO2, Faculté de Pharmacie, Aix-Marseille Université, Marseille, France,[1] and INSERM UMR 600-CNRS UMR 6212, Adhésion cellulaire et inflammation, Aix-Marseille Université, Marseille, France[2]

Received 30 July 2008/Returned for modification 1 October 2008/Accepted 12 May 2009

NADPH oxidase 1 (Nox1) is expressed mainly in colon epithelial cells and produces superoxide ions as a primary function. We showed that Nox1 knockdown inhibits directional persistence of migration on collagen I. This paper dissects the mechanism by which Nox1 affects the direction of colonic epithelial cell migration in a two-dimensional model. Transient activation of Nox1 during cell spreading on collagen 1 temporarily inactivated RhoA and led to efficient exportation of α2β1 integrin to the cell surface, which supported persistent directed migration. Nox1 knockdown led to a loss of directional migration which takes place through a RhoA-dependent α2/α3 integrin switch. Transient RhoA overactivation upon Nox1 inhibition led to transient cytoskeletal reorganization and increased cell-matrix contact associated with a stable increase in α3 integrin cell surface expression. Blocking of α3 integrin completely reversed the loss of directional persistence of migration. In this model, Nox1 would represent a switch between random and directional migration through RhoA-dependent integrin cell surface expression modulation.

The two well-recognized defining hallmarks of cancer are uncontrolled proliferation and invasion (14). The conversion of a static primary tumor into an invasive disseminating metastasis involves an enhanced migratory ability of the tumor cells. Tumor cells use migration mechanisms that are similar, if not identical, to those that occur in normal cells during physiological processes such as embryonic morphogenesis, wound healing, and immune-cell trafficking (10). To migrate, cells must acquire a spatial asymmetry that enables them to turn intracellularly generated forces into net cell body translocation. Dynamic assembly and disassembly of integrin-mediated adhesion and cytoskeletal reorganization are necessary for efficient migration (29). Integrins are heterodimeric integral membrane proteins composed of an α chain and a β chain. Depending on the cell type and extracellular matrix (ECM) substrate, focal contact assembly and migration can be regulated by different integrins. Collagen receptors include α1β1, α2β1, and α3β1 integrins. α1β1 and α3β1 integrins also bind laminin and have less affinity for collagen than does integrin α2β1 (47). The intrinsic propensity of cells to continue migrating in the same direction without turning is closely related to integrin/cytoskeletal interaction, which is known to regulate tractional forces, resulting in modulation of the speed and direction of cell migration (33). Interestingly, different integrin-ECM associations might have opposite effects on the regulation of the directionality of migration. Danen et al. have shown that adhesion to fibronectin by αvβ3 promotes persistent migration through activation of the actin-severing protein cofilin, which results in a polarized phenotype with a single broad lamellipod at the leading edge. In contrast, adhesion to fibronectin by α5β1 instead leads to phosphorylation/inactivation of cofilin and these cells fail to polarize their cytoskeleton and adopt a random/nonpersistent mode of migration (5). Members of the Rho GTPase family (including RhoA, Rac1, and Cdc42) are known as key modulators of cytoskeletal dynamics that occur during cell migration (37). RhoA regulates stress fiber and focal adhesion assembly, Rac regulates the formation of lamellipodial protrusions and membrane ruffles, and Cdc42 triggers filopodial extensions at the cell periphery (13).

One of the earliest characterized functions of the Rho GTPase Rac was regulation of the activity of the NADPH oxidase complex in phagocytic cells to produce reactive oxygen species (ROS) (1, 19). Moreover, it has been shown that Rac-dependent ROS production leads to downregulation of RhoA through oxidative inactivation of the low-molecular-weight (LMW) protein tyrosine phosphatase (PTP) and the subsequent activation of p190RhoGAP (31). ROS are also known to directly affect important regulators of cell migration such as PTEN, FAK, or Src (4, 20, 22). ROS are generated in cells from several sources, including the mitochondrial respiratory chain, xanthine oxidase, cytochrome P450, nitric oxide synthase, and NADPH oxidase. The seven known human catalytic subunits of NADPH oxidase include Nox1 to -5 and Duox1 and -2, with Nox2 (gp91phox) being the founding member (21). These oxidases participate in several adaptive functions, ranging from mitogenesis to immune cell signaling (11). A growing body of data points to a key role for ROS production by NADPH oxidase in the control of cell migration and cytoskeletal reorganization (30, 44). Among NADPH oxidase ho-

* Corresponding author. Mailing address: INSERM UMR 911, Centre de Recherche en Oncologie biologique et en Oncopharmacologie, Faculté de Pharmacie, Aix-Marseille Université, 27 Boulevard Jean Moulin, 13385 Marseille Cedex 5, France. Phone: (33) 491 835 627. Fax: (33) 491 835 506. E-mail: hkovacic@univmed.fr.

† Supplemental material for this article may be found at http://mcb.asm.org/.

▽ Published ahead of print on 18 May 2009.

mologs, Nox1 has been detected in different cell types, with major expression in vascular smooth muscle cells and colonic epithelial cells (42). Nox1 involvement in the control of cytoskeletal organization and cellular migration has been only recently reported. Shinohara et al. demonstrated that oncogenic Ras transformation involves Nox1-dependent signaling and leads to inactivation of RhoA. Abrogation of Nox1-dependent ROS production by diphenyleneiodonium (DPI) or small interfering RNA restores RhoA activation and actin stress fiber formation (41). More recently, several groups have highlighted a key role of Nox1 in the control of growth factor-induced migration (16, 38, 40). Cancer cells probably undergo random migration during metastasis, but their migration can be directed by cytokine gradients and/or associated with ECM fibers (29, 55). In a recent report, we showed that Nox1 downregulation decreased the persistence of colonic adenocarcinoma cell migration over collagen I (Col-I) without affecting either the mean velocity or the total distance of migration.

In the present study, we investigated the molecular mechanism by which Nox1-dependent ROS production controls the directionality of migration of colonic adenocarcinoma cells. We showed that Nox1-dependent ROS production, which occurs during cell spreading after 4 h of adhesion to Col-I, transiently inhibited RhoA activity. Nox1 inhibition during cell spreading led to a transient increase in cell-matrix contact and initiated a sustained decrease in $\alpha2\beta1$ integrin cell surface expression, which was compensated for by an increase in $\alpha3$ integrin cell surface expression. While Nox1-dependent RhoA inhibition was transient, the observed $\alpha2/\alpha3$ integrin switch was sustained over 24 h. The loss of directionality observed in cell migration upon Nox1 inhibition may be reversed by $\alpha3$ integrin blockade. This work shows that Nox1 is involved in the control of integrin surface expression during migration on Col-I, which is critical for persistent directed migration through transient modulation of a RhoA/ROCK-dependent pathway.

MATERIALS AND METHODS

Materials and reagents. Fetal bovine serum, trypsin-EDTA, Dulbecco's modified Eagle's medium, and sodium pyruvate were obtained from Gibco-BRL (Invitrogen Corporation, Scotland, United Kingdom). Diogenes was obtained from National Diagnostics (Atlanta, GA). Mouse monoclonal anti-$\alpha1$ (FB12), mouse monoclonal anti-$\alpha2\beta1$ (Gi9), rabbit anti-$\alpha2$ (AB1944), rabbit anti-$\alpha3$ (AB1920), rabbit anti-phospho-MLC (MLC is myosin light chain), and rabbit anticofilin antibodies were obtained from Millipore (Guyancourt, France). Rabbit monoclonal anti-phospho-cofilin antibody (77G2) was obtained from Ozyme (Saint-Quentin-en-Yvelines, France). DGEA (integrin $\alpha2\beta1$ recognition sequence Asp-Gly-Glu-Ala, an $\alpha2$-blocking peptide) was obtained from Euromedex (Souffelweyersheim, France). Mouse monoclonal anti-$\alpha3$ antibody (C3 [VLA3]) was obtained from Beckman Coulter (Villepinte, France). Mouse anti-RhoA monoclonal antibody was obtained from Tebu-Bio SA (Le Perray-en-Yvelines, France). Rabbit anti-p190RhoGAP antibody and mouse anti-MLC monoclonal antibody and mouse antipaxillin, rhodamine-phalloidin, and 3-aminopropyltriethoxysilane monoclonal antibodies were obtained from Sigma-Aldrich (Saint-Quentin-Fallavier, France). Y27632 was obtained from VWR International (Strasbourg, France). The RhoA G-LISA Activation Assay absorbance-based kit was obtained from Cytoskeleton (Denver, CO).

Cell culture and transfections. HT29-D4 cells, originally derived from the HT29 colon adenocarcinoma cell line (9), were cultured in Dulbecco's modified Eagle's medium supplemented with 10% fetal bovine serum, 25 mM D-glucose, sodium pyruvate (1%, vol/vol), and L-glutamine (2 mM). Cells were harvested in single-cell suspension by treatment with trypsin-EDTA and subsequently transfected by Amaxa Nucleofector according to the manufacturer's protocol. pAlpha2-EGFP-N3 overexpressing an $\alpha2$-green fluorescent protein (GFP) fusion protein was kindly provided by J. Ivaska (University of Turku, Turku, Finland) (35). Control plasmid pRk5 and plasmid pRk5-RhoA^{V14} were kindly given by Alan Hall (Sloan-Kettering Cancer Center). Nox1 short hairpin RNA (shRNA) was previously validated and described (6, 38). Transfected cells were serum depleted for 48 h, detached with 0.25% trypsin, and seeded onto Col-I-precoated plates (10 μg/ml). The efficiency of Nox1 shRNA compared to control shRNA was evaluated in all experiments involving Nox1 shRNA (see Fig. S1 in the supplemental material).

Migration assay. At 24 h after passage, cells were serum depleted for 48 h, trypsinized, and then seeded onto Col-I-precoated 24-well plates at low confluence (25×10^3 cells/cm^2). Analysis of cell migration at 37°C was performed with an inverted Leica DMIRB microscope at $\times10$ magnification. Time-lapse recording started 2 h after plating (end of the adhesion phase). Three fields per well were imaged and followed at 10-min intervals for 8 h with a cooled charge-coupled device (CCD) video camera operated by Metamorph image analysis software (Princeton Instruments, Evry, France). Each individual cell displacement was determined with the "track object" function in the Metamorph software. For each of at least 45 independent cells, the net displacement between two images was determined from time-lapse movies. These measurements allow calculation of the total migration distance, distance to the origin, rate of migration, and directional persistence of cell migration. The total migration distance represents the sum of the net displacements between measurements over a period of 8 h. The distance to the origin was determined as the net displacement between the initial position and the final position observed during an 8-h period. The mean directional persistence was calculated as the average ratio of the distance to the origin for at least 45 individual cells during an 8-h period and the total migration distance. In order to follow the variation of the rate and persistence of migration over time, we calculated the instantaneous velocity and instantaneous persistence. The mean instantaneous velocity was calculated for at least 45 individual cells as the net displacement of cells between two consecutive frames divided by the time (10 min) and smoothed by adjacent averaging of five frames over the 8 h of migration. Mean instantaneous persistence was calculated as previously described (34), with modifications. Briefly, for every cell in each consecutive frame (n), the net displacement (D) over a five-frame interval [(n; $n + 5$)] was divided by the cumulative displacement (T) over the five-frame interval. The instantaneous persistence plotted over time represents the average of at least 45 individual cells.

Flow cytometry. Cell surface expression of integrin subunits in HT29-D4 cells was determined by flow cytometry. Cells were incubated with different inhibitors or vehicles for 30 min, harvested with trypsin/EDTA (0.25%/0.53 mM), and resuspended in serum-depleted medium containing 1% (wt/vol) BSA. Cell suspensions (2×10^6 cells/ml) were incubated for 1 h at 4°C in solutions containing a saturating concentration of anti-integrin antibodies (10 μg/ml). Cells were rinsed three times with ice-cold phosphate-buffered saline (PBS) containing 1% BSA and then incubated for 45 min at 4°C in the dark with an excess of goat anti-mouse fluorescein isothiocyanate-conjugated antibody. After washing, cells were fixed in 1% paraformaldehyde and analyzed by injection onto a FACScan flow cytometer (Becton Dickinson, San Diego, CA).

IRM. Interference reflection microscopy (IRM) is based on the interference of light reflected from closely apposed surfaces to provide an image containing information about the separation of those surfaces within a 100-nm range. Dark zones on IRM images are indicative of cell surface attachment (48). Before cell seeding, 9-cm^2 glass slides were treated with 3-aminopropyltriethoxysilane and then incubated with 0.25% glutaraldehyde. The glass slides were then coated with Col-I, and nonspecific aminosilane binding sites were blocked with ethanolamine. At 24 h after passage, cells were serum depleted for 48 h, trypsinized, and then seeded onto Col-I-precoated 9-cm^2 glass slides at low confluence (25×10^3 cells/cm^2). Chambers were deposited on an Axiovert 135 inverted microscope (Zeiss, Jena, Germany) equipped with a heating stage (TRZ 3700) set at 37°C. IRM was performed with an antiflex objective ($\times63$ magnification, 1.25 numerical aperture). Images were obtained with a Hamamatsu C4742-95-10 CCD camera (10-bit accuracy) driven by HIPIC software. Each greyscale image obtained was 8 bit converted and subjected to background subtraction to limit uneven illumination across the field of view with ImageJ software (24). The image threshold was set at a value of 90 (on a scale of 0 to 255). To express the variation in cell-matrix contact, the integrated densities of at least 45 cells (from different fields of view) were calculated. Results representative of three independent experiments were expressed as the relative increase (percent) over the value obtained for control cells.

Immunofluorescence experiments. At 24 h after passage, cells were serum depleted for 48 h, trypsinized, and then seeded onto Col-I-precoated glass coverslips. After the end of the spreading phase (at 3.5 h) or at 5.5 h, cells were incubated with DPI for 30 min and then fixed in 3.7% formaldehyde in PBS,

containing 1 mM $MgCl_2$ and 0.5 mM $CaCl_2$. Cells were permeabilized in 0.2% Triton X-100 for 5 min and blocked with 3% bovine serum albumin (BSA) in PBS. Cells were stained for actin with rhodamine-phalloidin. For immunofluorescence assay, cells were labeled overnight at 4°C with primary antibodies at 5 μg/ml and then with the appropriate fluorescent secondary antibody. For integrin staining, cells were observed under an oil immersion 100× Plan-Fluotar objective on an inverted Leica DMIRB microscope and photographed with a CoolSnapFx CCD camera and Metamorph software. Dual labeling for actin and paxillin was performed with a 63× HCX PL APO oil objective on a Leica SP5 confocal microscope.

Measurement of ROS. ROS generation was measured by lucigenin (not shown) and Diogenes reagent. As described previously (6), after incubation of cells on Col-I for the desired time in 96-well plates (25×10^3 cells/well), luminescence was detected by a Fluoroscan Ascent FL fluorimeter (Labsystems, France). The detected signal was assessed once a minute for 45 min. Results represent the integration of the signal for 45 min and associated with the intermediate time of measurement. All measurements were performed at 37°C.

Preparation of whole-cell lysates. Cells were lysed in radioimmunoprecipitation assay buffer (50 mM Tris-HCl, 150 mM NaCl, 0.1% sodium deoxycholate, 4 mM EDTA, 50 mM NaF, 1 mM sodium orthovanadate, 10 mM sodium pyrophosphate, 1 mM phenylmethylsulfonyl fluoride [PMSF], 1 μg/ml leupeptin, 1 μg/ml aprotinin) and centrifuged for 10 min at $10,000 \times g$. The supernatant protein concentration was determined with the bicinchoninic acid assay (Perbio Sciences, Brebieres, France) by following the manufacturer's instructions.

Subcellular fractionation. Adherent cells were washed and treated with ice-cold hypotonic lysis buffer (10 mM Tris [pH 7.4], 1.5 mM $MgCl_2$, 5 mM KCl, 1 mM dithiothreitol, 0.2 mM sodium vanadate, 1 mM PMSF, 1 μg/ml aprotinin, 1 μg/ml leupeptin) and then scraped. Cell lysates were homogenized and then centrifuged at 2,000 rpm for 3 min to pellet nuclei and intact cells, and supernatants were then spun at 15,000 rpm at 4°C for 30 min in a refrigerated centrifuge to sediment the particulate fraction. The cytosol-containing supernatant was removed, and the particulate fraction was gently washed with hypotonic lysis buffer (7).

Western blotting. Equal amounts of protein from lysates were resolved by 10% sodium dodecyl sulfate-polyacrylamide gel electrophoresis (SDS-PAGE) and transferred to Hybond ECL nitrocellulose membranes (Amersham Pharmacia Biotech, France). Membranes were blocked in low-fat milk and incubated with primary antibodies overnight at 4°C. Membranes were washed and subsequently incubated for 1 h with anti-mouse, anti-rabbit, or anti-goat immunoglobulin–horseradish peroxidase. Proteins were visualized with an enhanced chemiluminescence detection kit (Amersham Pharmacia Biotech, France).

Pulldown assay of activated RhoA. After incubation of cells on Col-I for the desired time, HT29-D4 cells were lysed in lysis buffer (50 mM Tris-HCl [pH 7.2], 100 mM NaCl, 5 mM $MgCl_2$, 1% Nonidet P-40, 1 mM dithiothreitol, 10% glycerol, 1 mM PMSF) and the lysates were incubated with glutathione *S*-transferase–Rhotekin Rho binding domain coupled to glutathione-Sepharose for 120 min at 4°C. After extensive washing with lysis buffer, the proteins retained on the resins were analyzed by immunoblotting with anti-RhoA antibody.

RhoA activation assay kit. Nox1 shRNA- and control shRNA-transfected cells were seeded onto Col-I. After 3.5 h, cells were treated with DPI (10 μM) for 30 min. RhoA GTPase activation was determined with the absorbance-based RhoA G-LISA activation assay according to the manufacturer's protocol.

Statistical analysis. Results are expressed as means ± standard errors from at least three independent experiments. Statistical analysis was performed by the unpaired Student *t* test. A value of $P < 0.05$ was considered statistically significant.

RESULTS

Nox1 modulates the RhoA/ROCK pathway during cell spreading. We previously showed that ROS produced after 4 h of adhesion to Col-I in HT29-D4 cells are inhibited by DPI, the flavoprotein inhibitor classically used to inhibit NADPH oxidase. We and others have shown that Nox1 is the only Nox homologue detected in HT29 cells (6, 12). By using shRNA directed against Nox1, we confirmed that the DPI effect relies on Nox1 inhibition in our experimental model (6). We showed that the transient Nox1-dependent superoxide production affects the α2 integrin expression level and cell migration direction (6, 38). The GTPase RhoA is a well-known regulator of actin stress fiber formation and focal adhesion assembly (13) and a downstream target for NADPH oxidase and ROS (31, 41). Results in Fig. 1A show simultaneous measurement of superoxide production and RhoA activation by Rho pulldown assay during the time course of cell adhesion to Col-I. RhoA activation was not seen in suspended cells and was first detected after 2 h of adhesion. RhoA activation decreased after 4 h of adhesion compared to 2 h of adhesion. This decrease was concomitant with the increase in Nox1-dependent superoxide production. RhoA activation increased again after 6 h of adhesion, while Nox1-dependent superoxide production was decreased. NADPH oxidase inhibition by addition of DPI at the onset of ROS production increased RhoA activation compared to that in the control, while DPI addition after the transient ROS production did not affect RhoA activation compared to that in the control (Fig. 1A). The immunoblot assay for Nox1 in Fig. 1B shows that Nox1 shRNA decreased the Nox1 expression level by more than 80% compared to control shRNA expression, as previously validated and confirmed at the mRNA level (6). A 3.5-fold increase in the Rho-GTP level was observed in Nox1 shRNA-transfected cells compared to that in the control after 4 h of adhesion to Col-I, as quantified by the G-LISA active-RhoA detection kit (Fig. 1C). DPI addition to Nox1 shRNA-transfected cells did not produce a further increase in the Rho-GTP level, confirming that the DPI effect was due to Nox1 inhibition. These data suggest that Nox1-dependent ROS production downregulates RhoA activity during HT29-D4 spreading and migration on Col-I. We next examined the signaling mechanism linking Nox1 to the negative regulation of RhoA activity through p190RhoGAP modulation. p190RhoGAP is a GTPase-activating protein that acts as an inhibitor of RhoA activity. Upon its tyrosine phosphorylation, p190RhoGAP associates with p120RasGAP and translocates to the plasma membrane, which correlates with the increased Rho-inhibiting activity of p190RhoGAP (3). We explored the impact of Nox1-dependent ROS production on p190RhoGAP activity by assessing the level of membrane-translocated p190RhoGAP. Immunoblot assays of the membrane fraction presented in Fig. 1D show that p190RhoGAP membrane recruitment occurred after 4 h of adhesion, consistent with the decrease in the Rho-GTP level observed at that time. Suppression of Nox1-dependent superoxide by DPI or Nox1 shRNA decreased p190RhoGAP membrane recruitment at the onset of ROS production compared to that of the respective control. The p190RhoGAP level was not affected by DPI treatment or by Nox1 shRNA in the cytosolic fraction, suggesting that only a small amount of p190RhoGAP was associated with the plasma membrane (data not shown). These results are consistent with the detected increase in RhoA activity upon Nox1 inhibition under the same conditions. Morphological changes induced by Nox1 inhibition were observed by immunofluorescence staining by confocal dual labeling of paxillin and actin. Figure 1E shows that DPI-treated cells after 4 h of adhesion displayed a large paxillin patch at the cell periphery and actin stress fibers in the cellular body. In contrast, control cells after 4 h of adhesion and DPI-treated cells and control cells after 6 h of adhesion presented a smaller paxillin patch and less polymerized actin. The involvement of Nox1 in the control of cell-matrix contact during spreading on Col-I was studied by IRM. IRM is classically used to study cell

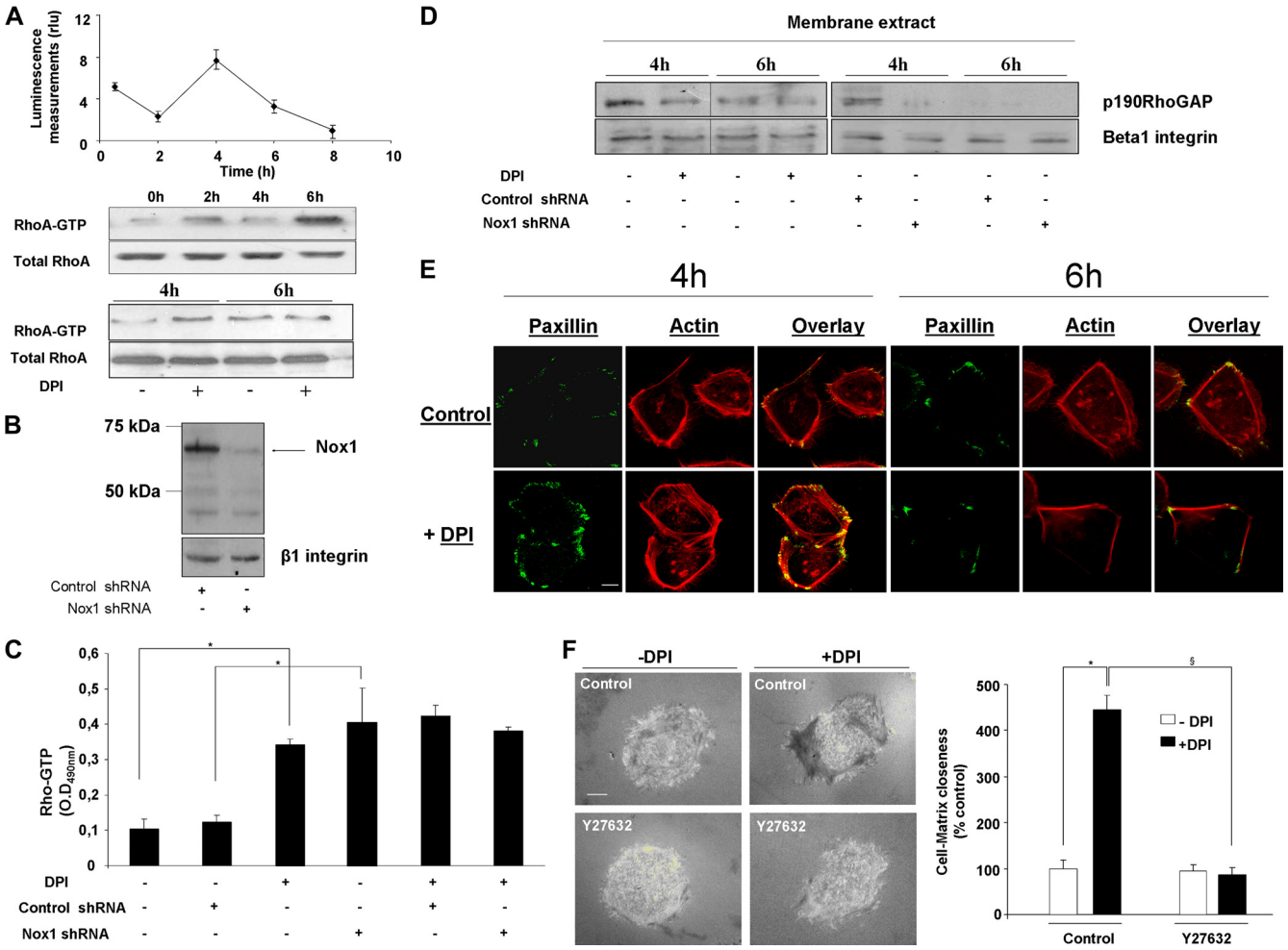

FIG. 1. Nox1-dependent downregulation of the RhoA-GTP level is mediated by p190RhoGAP and affects cell-matrix contact during adhesion to Col-I. (A) Superoxide production was measured over adhesion time by chemiluminescence. Data are presented as means ± standard errors. The RhoA-GTP level over adhesion time was determined by a Western blot pulldown assay with glutathione *S*-transferase–Rhotekin Rho binding domain beads. A Western blot assay of the total RhoA level was used as a loading control. DPI (10 μM) or vehicle was added 30 min before 4 or 6 h of adhesion to Col-I. (B) Nox1 shRNA efficiency compared to that of control shRNA was evaluated by immunoblot assay. β1 integrin was used as a loading control. (C) The RhoA-GTP level in cells transfected with Nox1 or a control shRNA and seeded for 4 h on Col-I was assessed by using the RhoA G-LISA Activation Assay according to the manufacturer's instructions. DPI (10 μM) or vehicle was added 30 min before cell lysis. Data are presented as means ± standard errors. *, $P < 0.05$ compared with the control. $O.D_{490nm}$, optical density at 490 nm. (D) Membrane translocation of p190RhoGAP was assessed by Western blot assay of the particulate fraction isolated from cells treated with DPI or transfected with Nox1 or control shRNA. DPI (10 μM) or vehicle was added 30 min before cell lysis. (E) Fluorescence staining for actin (rhodamine phalloidin) and paxillin was performed on cells seeded for 4 or 6 h onto glass coverslips precoated with Col-I. DPI treatment was applied 30 min before fixation. Sequential image acquisition was performed with a Leica confocal microscope. Scale bar, 4 μm. (F) Cells were seeded onto Col-I-precoated glass coverslips and treated at 3.5 h for 30 min with DPI (10 μM), the ROCK inhibitor Y27632 (10 μM), or both. Cell-matrix contact was analyzed by IRM as described in Materials and Methods. The increase in cell-matrix contact (increase in the dark zone) was expressed as a percentage of that of untreated control cells. Data are presented as means ± standard errors. *, $P < 0.05$ compared with the control; §, $P < 0.05$ compared with DPI-treated cells.

adhesion by measuring the separation between the cell membrane and the ECM coating a glass surface to which the cell is attached (8). The cell-ECM distance was linked to pixel intensity by using a continuum between black pixels representative of a close cell-ECM interaction and white pixels representative of a large distance between the cell and the ECM (see Materials and Methods). Inhibition of transient Nox1-dependent ROS production by DPI increased cell-matrix contact compared to that in the control (440% ± 29% versus 100% ± 16%, respectively; Fig. 1F). The impact of the downstream RhoA effector ROCK was assessed with the pharmacological inhibitor Y27632 (10 μM). ROCK inhibition fully reversed the transient DPI increase in cell-matrix contact observed after 4 h of adhesion to Col-I (Fig. 1F). In addition, Y27632 did not affect the Nox1-dependent ROS production, confirming that the RhoA/ROCK pathway was downstream of Nox1 activation (not shown). These results suggest that Nox1 inhibition during the spreading phase leads to a reinforcement of cell anchorage through the RhoA/ROCK pathway.

Nox1-dependent ROS production controls cell adhesiveness through the modulation of cell surface α2/α3 integrin expression. We previously reported that Nox1 controls α2 integrin

subunit membrane availability (38). The reinforcement of cell-matrix contact during Nox1 inhibition observed in the present study (Fig. 1) suggested that the surface expression or activation status of other integrins might have been affected. Besides α2β1 integrin, HT29-D4 cells express other α subunits involved in the binding of Col-I in association with β1 (i.e., α1and α3 integrin subunits). Quantification of those α subunit surface expression levels by flow cytometry after 24 h of adhesion to Col-I showed median fluorescence levels of 45 ± 5, 232 ± 25, and 200 ± 21 for the α1, α2, and α3 integrin subunits in HT29-D4 control cells, respectively. The median fluorescence obtained without primary antibody was 26 ± 3. Under DPI treatment or in Nox1 shRNA-treated cells compared to the shRNA control, α1 cell surface expression remained constant, while α3 integrin cell surface expression increased (100% ± 9% versus 140% ± 9% for the control versus DPI treatment) concomitant with a decrease in α2 integrin cell surface expression (100% ± 9% versus 60% ± 8% for the control versus DPI treatment). We qualified this effect induced by Nox1 inhibition as a "α2/α3 integrin subunit switch." We then measured the integrin cell surface expression upon Nox1 inhibition directly at the onset of the transient Nox1-dependent ROS production after 4 h of adhesion to Col-I. DPI was added 3.5 h after adhesion to Col-I, and integrin cell surface expression was measured 30 min after treatment. Results presented in Fig. 2B show that the α2/α3 integrin subunit switch was initiated at the onset of transient Nox1-dependent ROS production. Under the same conditions, α1 and β1 integrin cell surface expression did not change in DPI-treated cells compared to that in controls. Moreover, Nox1 shRNA expression had the same effect as DPI on α2 and α3 integrin cell surface expression. DPI addition to Nox1 shRNA-transfected cells did not further decrease α2 integrin cell surface expression or increase the α3 integrin cell surface expression level (Fig. 2C). Induction of the α2/α3 integrin subunit switch took place after 30 min of Nox1-dependent ROS production inhibition, suggesting posttranslational regulation rather than transcriptional control of α2 expression. HT29-D4 cells transfected with the pAlpha2-EGFP-N3 construct, which overexpress an α2-GFP fusion protein under the control of the cytomegalovirus promoter, exhibited an α2β1 integrin cell surface expression level higher than that of control transfected cells (146% ± 8% versus 100% ± 7%, respectively). Interestingly, DPI decreased both control and overexpressed α2 integrin subunit cell surface expression, confirming that Nox1 short-term regulation of α2 integrin subunit cell surface expression is not transcriptional (Fig. 2D). To prove the link between cell-matrix contact modification and the α2/α3 integrin switch, we used an α1, α2, and α3 integrin subunit-blocking approach. Results presented in Fig. 3 show that whereas cell treatment with the α3 integrin-blocking antibody completely reversed the DPI-dependent increase in cell-matrix contact, blocking α2 integrin by DGEA was ineffective. Since Nox1 inhibition did not affect the α1 integrin, we used the α1 integrin-blocking antibody as a nonrelevant control antibody. As expected, α1 integrin inhibition did not reverse the DPI effect. These findings suggest that the increase in cell-matrix contact induced by Nox1 inhibition after 4 h of adhesion is exclusively due to the DPI-mediated increase in α3 integrin cell surface expression. This finding was confirmed by the confocal dual labeling of paxillin and actin upon 30 min of treatment at 3.5 h of adhesion to Col-I with DPI, α3-blocking antibody, or both. Indeed, results presented in Fig. 3B show that blocking α3 integrin inhibited stress fiber formation and focal adhesion assembly upon DPI addition, suggesting that α3 integrin is essential for the DPI-induced stabilization of actin fibers and focal adhesion assembly.

RhoA/ROCK pathway controls Nox1-dependent integrin switch through p38 mitogen-activated protein kinase (MAPK) modulation. Confirming the involvement of α3 integrin in Nox1 inhibition, the peripheral distribution of α2 integrin was not affected whereas α3 integrin clusters were detected in DPI-treated cells (Fig. 4A). Expression of a constitutively activated mutant form of RhoA, $RhoA^{V14}$, induces the α2/α3 integrin subunit switch after 4 h of adhesion to Col-I, and DPI did not further modify integrin cell surface expression (Fig. 4B). This suggests that RhoA acts downstream of Nox1 to modulate the α2/α3 integrin subunit switch. In addition, ROCK inhibition by Y27632 (10 μM) completely blocked the DPI-mediated α2/α3 integrin switch (Fig. 4D). We previously reported that DPI and Nox1 shRNA decrease the total α2 integrin subunit protein level (38). We addressed the possible modification of the total α2 and α3 integrin subunit protein level by the RhoA/ROCK pathway during adhesion to Col-I. Immunoblot assays presented in the lower inset of Fig. 4B and in Fig. 4C show that neither $RhoA^{V14}$ overexpression nor Y27632 affected the α2 or α3 integrin subunit protein level after 4 and 24 h of adhesion to Col-I. DPI and Nox1 shRNA did not modify the α2 or α3 total integrin subunit protein level after 4 h of adhesion, while they inhibited only the α2 total integrin subunit protein level after 24 h of adhesion to Col-I. These results suggest that the $RhoA^{V14}$-mediated α2/α3 integrin subunit switch downstream of Nox1 inhibition is not a consequence of transcriptional regulation. In addition, these data show that during adhesion to Col-I, Nox1 controls α2 integrin subunit availability through two independent pathways. One pathway affects the total α2 integrin subunit protein level, while the other involves a RhoA/ROCK pathway and controls α2 integrin membrane availability.

In order to determine the downstream targets of the RhoA/ROCK pathway affected under Nox1 inhibition, we measured the phosphorylation levels of cofilin and MLC upon treatment with DPI at the onset of (4 h) or after transient Nox1 activation (6 h). Immunoblot assays presented in Fig. 5A show that at the onset of Nox1 activation, MLC was not phosphorylated whereas cofilin phosphorylation was detected. Inhibition of Nox1 activation by DPI increased the MLC phosphorylation level, while cofilin phosphorylation was not further increased by DPI addition. This increased MLC phosphorylation level is in agreement with the detected increase in stress fiber formation and focal adhesion assembly observed upon Nox1 inhibition. In contrast, DPI addition when Nox1 was not activated did not affect the activity of either MLC or cofilin. We confirmed that the increased MLC phosphorylation induced by DPI was linked to Nox1 inhibition since Nox1 shRNA induced the same effect (Fig. 5A). MLC phosphorylation induced by the pharmacological inhibition or the knockout of Nox1 was reversed by the ROCK inhibitor Y27632 but not by an anti-α3 integrin blocking antibody. These results suggest that MLC phosphorylation is a consequence not of α3 integrin-mediated outside-in signaling but downstream ROCK activation. More-

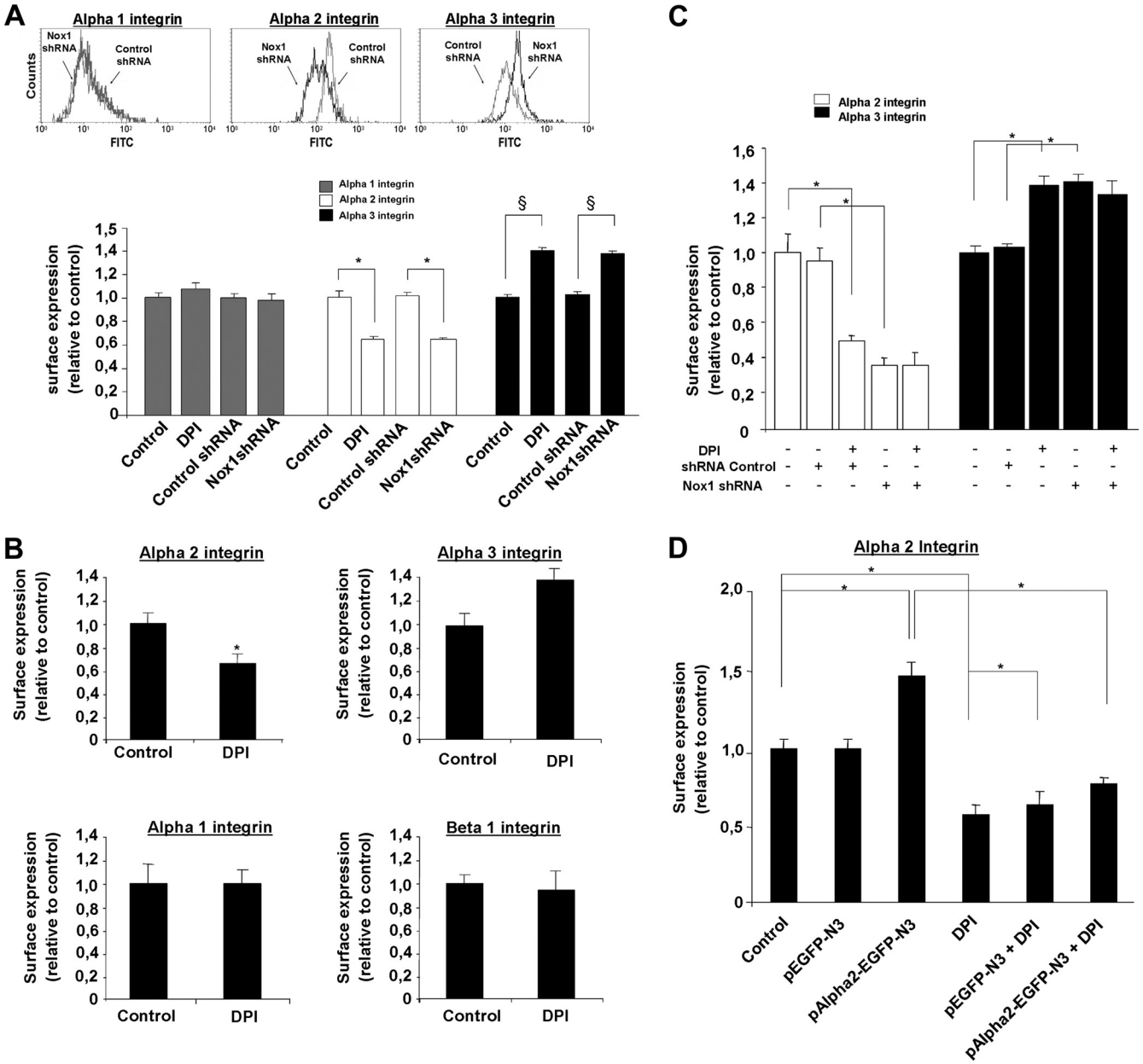

FIG. 2. Nox1-dependent ROS production controls cell surface α2/α3 integrin expression. Cell surface expression of integrins after adhesion to Col-I was assessed by flow cytometry. Data are presented as means ± standard errors. (A) Cell surface expression of α1, α2, and α3 integrins was assessed after 24 h of adhesion to Col-I. Cells were transfected with either Nox1 shRNA or control shRNA or left untransfected and treated with DPI (10 μM) after 2 h of adhesion. *, $P < 0.05$ compared with control α2; §, $P < 0.05$ compared with control α3. (B) Cell surface expression of α1, α2, α3, and β1 integrins was assessed after 4 h of adhesion (the onset of Nox1 activation). DPI (10 μM) or vehicle was added 30 min prior to measurement. *, $P < 0.05$ compared with the control. (C) Cell surface expression of α2/α3 integrins was assessed on Nox1 shRNA-transfected and control transfected cells treated with DPI (10 μM) or vehicle. *, $P < 0.05$ compared with the control. (D) Cell surface expression of α2 integrin was assessed after 4 h of adhesion on pAlpha2-EGFP-N3-transfected (overexpressing an α2-GFP fusion protein) or pEGFP-N3-transfected cells treated with DPI (10 μM) or vehicle for 30 min prior to measurement. *, $P < 0.05$ compared with the control.

over, blebbistatin, an inhibitor of actin-myosin II interaction, did not affect or reverse the DPI-induced integrin switch, suggesting that MLC phosphorylation and the subsequent actin stress fiber formation are concomitant with the integrin switch. We previously reported that membrane α2 integrin subunit availability was affected by p38 MAPK inhibition (38). The follow-up of p38 MAPK phosphorylation after 4 h of adhesion to Col-I showed that DPI inhibited p38 MAPK phosphorylation (Fig. 5B). Y27632 alone did not change the p38 MAPK phosphorylation level but blocked the inhibition induced by DPI. A similar reversion of p38 MAPK phosphorylation by Y27632 was observed in $RhoA^{V14}$-transfected cells. These results suggested that Nox1 inhibition affects p38 MAPK phosphorylation through the RhoA/ROCK pathway. SB203580, a

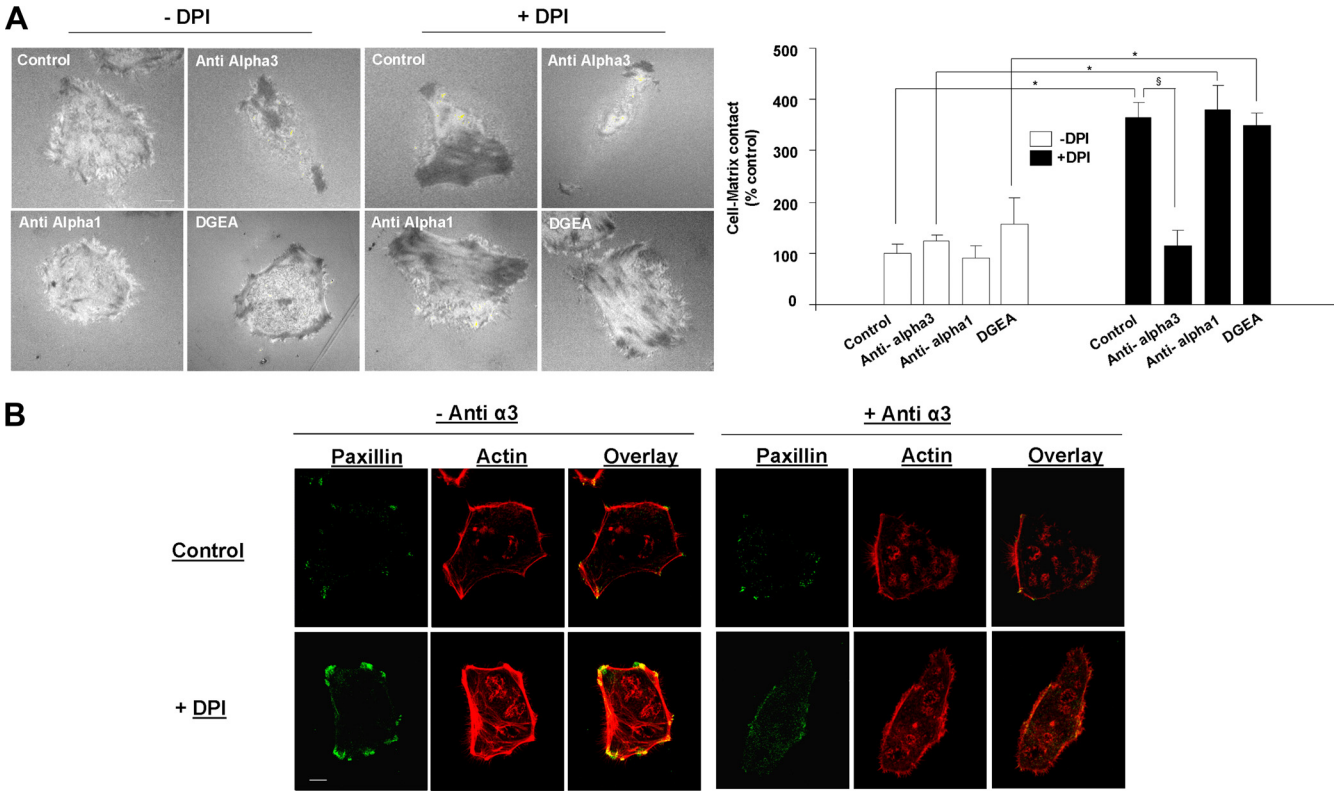

FIG. 3. Increased cell-matrix contact upon Nox1 inhibition relies on α3 integrin. (A) Cell-matrix contact was analyzed by IRM after 4 h of adhesion to Col-I. Treatment with DPI (10 μM), DGEA (α2-blocking peptide; 0.25 mM), and anti-α1 or anti-α3 blocking antibodies (10 μg/ml) was performed 30 min prior to measurement. Quantification of the area of contact (increase in pixel darkness and the number of dark pixels) was performed on at least 45 individual cells with ImageJ software. Data are presented as means ± standard errors. ⋆, $P < 0.05$ compared with non-DPI-treated cells; §, $P < 0.05$ compared with DPI-treated control cells. Bar, 4 μm. (B) Fluorescence staining for actin (rhodamine-phalloidin) and paxillin was performed on cells seeded for 4 h on Col-I and treated with DPI, anti-α3 blocking antibody, or both for 30 min before fixation. Sequential image acquisition was performed with a Leica confocal microscope. Scale bar, 4 μm.

pharmacological inhibitor of p38 MAPK, induced the integrin switch to the same extent as DPI did (Fig. 5C). In addition, SB203580 did not affect the phosphorylation level of MLC with or without DPI after 4 h of adhesion to Col-I (Fig. 5D). Finally, SB203580 did not affect the total α2 or α3 integrin subunit protein level after 4 and 24 h of adhesion to Col-I, confirming that the RhoA/ROCK/p38 MAPK pathway downstream of Nox1 is not involved in the long-term decrease of the total α2 integrin level. These results highlight a dual effect of ROCK activation, upon Nox1 inhibition, on both p38 MAPK/integrin surface expression and MLC/cytoskeletal reorganization. p38 MAPK is the major regulator of the integrin switch, while MLC phosphorylation would represent the key regulator of stress fibers in association with α3 integrin.

Nox1-dependent ROS production controls the directionality of cell migration on Col-I through the modulation of cell surface α2/α3 integrin expression. Nox1 knockdown by shRNA or inhibition by DPI affects the directional persistence of cell migration over Col-I. We have initially correlated this effect to a decrease in α2 integrin cell surface expression measured 24 h after adhesion (38). Comparison of α2 and α3 integrin subunit surface expression between the start and end of migration showed that α2 integrin cell surface expression increased during cell migration, while α3 integrin cell surface expression was not significantly affected (Fig. 6A). DPI blocked the increase in α2 integrin cell surface expression during migration while it increased α3 integrin cell surface expression. The analysis of the persistence of cell migration under Nox1 inhibition with or without integrin-specific blocking antibodies and peptides is reported in Fig. 6B. In a control experiment, directional persistence of migration was decreased by α2 integrin blockade and unaffected by α3 integrin blockade. During Nox1 inhibition, α2 integrin blockade did not further decrease or reverse the persistence of migration. In contrast, α3 integrin blockade fully reversed the persistence of migration compared to the control without DPI (Fig. 6B). In addition, under Nox1 inhibition, α3 blockade did not rescue α2 surface expression (not shown). Results presented in Fig. 6C confirm that ROCK is a downstream effector of Nox1 since Y27632 blocked the loss of migration persistence induced by DPI. Finally, the loss of migration persistence observed under p38 MAPK inhibition was reversed by an anti-α3 integrin blocking antibody. These results suggest that the loss of persistence of migration upon Nox1 inhibition is mainly mediated by the increase in cell surface expression of α3 integrin. We previously showed that upon Nox1 knockdown, the mean velocity and mean total distance of migration remained constant while the mean distance to the origin and the directional persistence of migration

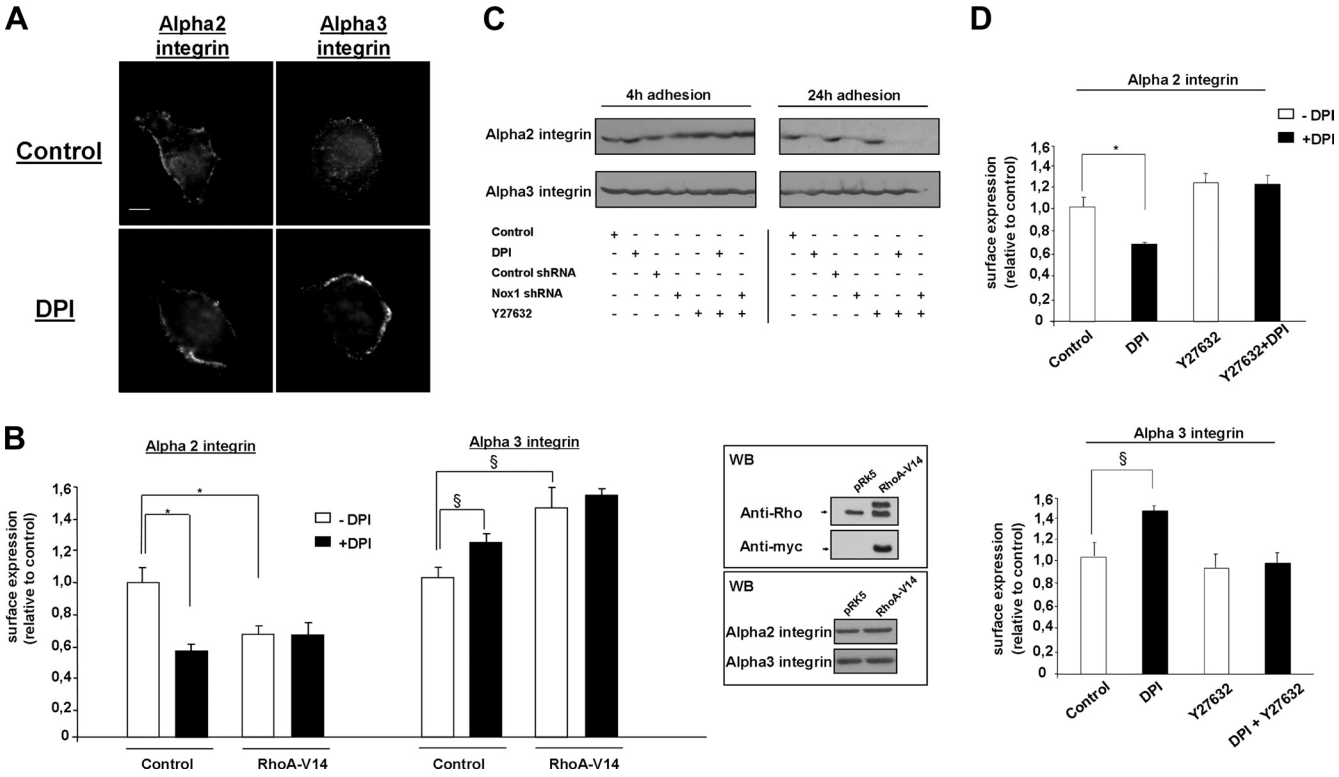

FIG. 4. Nox1 inhibition induces the α2/α3 integrin switch through the RhoA/ROCK pathway. (A) Cells were seeded onto Col-I-precoated plates for 4 h and treated with DPI (10 μM) or vehicle for 30 min before fixation. Cells were fixed, permeabilized, and subjected to immunofluorescence analysis with anti-α2 and anti-α3 integrin subunit antibodies. Scale bar, 4 μm. (B) Cell surface expression of α2 and α3 integrins after 4 h of adhesion to Col-I was assessed by flow cytometry on $RhoA^{V14}$-transfected and control transfected cells. Data are presented as means ± standard errors. *, $P < 0.05$ compared with α2; §, $P < 0.05$ compared with control α3. The upper inset represents the level of myc-tagged $RhoA^{V14}$ compared to that of endogenous RhoA determined by Western blot (WB) assay with primary anti-RhoA and anti-myc antibodies. The lower inset shows a Western blot assay with anti-α2 and anti-α3 integrin antibodies performed on $RhoA^{V14}$-transfected cells after 24 h of adhesion to Col-I. (C) Cells were transfected with either Nox1 shRNA or control shRNA or left untransfected and seeded onto Col-I. Cells were then treated at 3.5 h for 30 min with DPI (10 μM) or the ROCK inhibitor Y27632 (10 μM) or incubated for 24 h with the inhibitors shown. Lysates were prepared and analyzed by SDS-PAGE, followed by immunoblotting with anti-α2 or anti-α3 integrin antibodies. (D) Cell surface expression of α2 and α3 integrins after 4 h of adhesion to Col-I was assessed by flow cytometry on cells treated with DPI (10 μM), Y27632 (10 μM), or vehicle for 30 min before measurement. Data are presented as means ± standard errors. *, $P < 0.05$ compared with control α2; §, $P < 0.05$ compared with control α3.

decreased by 68 and 73%, respectively, compared to the control (38). As ROS modulation, RhoA activation, and integrin surface availability are subject to change during the time frame of migration analysis, we followed the instantaneous velocity and persistence during cell migration instead of the mean velocity and mean persistence. Under these conditions, a slowdown of velocity was observed during the transient overactivation of RhoA and initiation of the α2/α3 integrin switch by Nox1 inhibition. Then, an increased velocity was observed while RhoA activity returned to normal and the integrin switch was sustained (Fig. 6D). In contrast, inhibition of Nox1-dependent ROS production continuously decreases the instantaneous persistence over time. Since we showed that the RhoA activation levels were similar in control and DPI-treated cells after 6 h of adhesion, the cellular persistence of migration does not rely on the sole RhoA activation state. These results suggest that once induced by RhoA activation, the integrin switch is the major regulator of cellular migration persistence. Overall, these data are consistent with a transient impact of Nox1 on RhoA activity, leading to transient cytoskeletal reorganization and p38 phosphorylation, which increase α2 integrin subunit membrane availability, allowing efficient two-dimensional (2D) migration on Col-I (results are summarized in Fig. 7).

DISCUSSION

Cell motility requires fine regulation through Rho-GTPase signaling of the cytoskeleton and integrin network to control the speed and direction of cellular migration (37). Directional migration is involved in vivo in many physiopathological processes. Leukocytes and fibroblasts directionally moved toward the injury site, while directed migration in cancer cells increased the efficiency of extravasation during metastasis (29). A close relationship between ROS production and cell-matrix adhesion complexes, including integrins and cytoskeletal proteins, has been reported (43). In the present study, we investigated the molecular mechanism by which Nox1-dependent ROS production controls the direction of migration of colonic epithelial cells. We showed that Nox1-dependent ROS production transiently inhibits RhoA activity during cell spreading. This transient RhoA inhibition is necessary for α2β1 integrin externalization upon spreading on Col-I and for the further

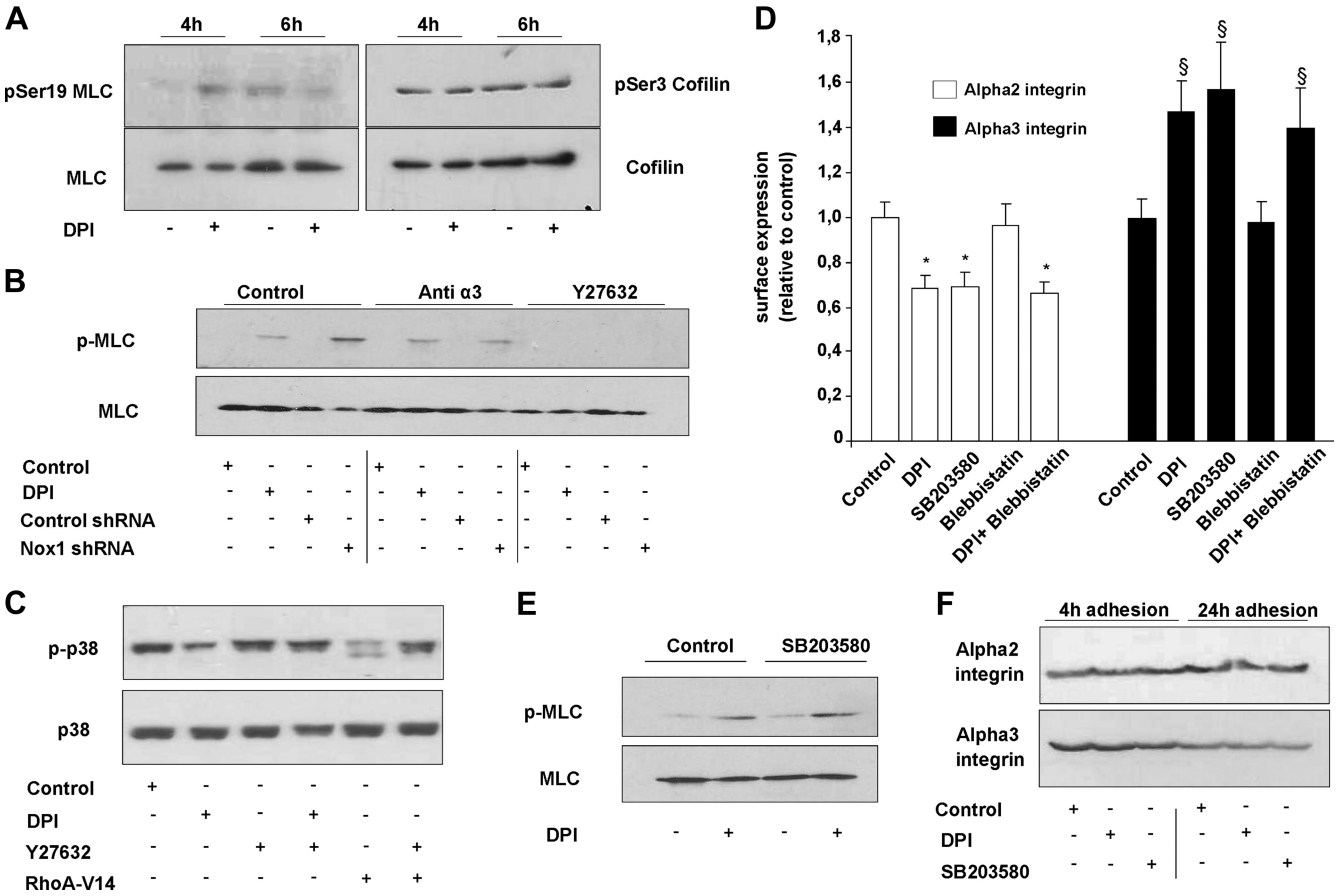

FIG. 5. Rho/ROCK pathway controls the Nox1-induced integrin switch through regulation of p38 MAPK phosphorylation. (A) Phosphorylation levels of cofilin and MLC were assessed by Western blot assay in cells seeded onto Col-I for 4 or 6 h. DPI (10 μM) or vehicle was added 30 min before cell lysis. Data are representative of three independent experiments. (B) Cells were transfected with either Nox1 shRNA or control shRNA or left untransfected and seeded onto Col-I. Cells were then treated at 3.5 h for 30 min with DPI (10 μM), the ROCK inhibitor Y27632 (10 μM), or anti-α3 antibody (10 μg/ml). Lysates were prepared and analyzed by SDS-PAGE, followed by immunoblotting with anti-pMLC or anti-MLC antibodies. (C) Cells were transfected with the RhoA-V14 construct or a control or left untransfected. Cells were then treated at 3.5 h for 30 min with vehicle, DPI (10 μM), the ROCK inhibitor Y27632 (10 μM), or both DPI and Y27632. Lysates were prepared and analyzed by SDS-PAGE, followed by immunoblotting with anti-phosphorylated p38 MAPK or anti-p38 MAPK antibodies. (D) Cell surface expression of α2 integrin was assessed after 4 h of adhesion to HT29-D4 cells treated with vehicle, DPI (10 μM), the p38 MAPK inhibitor SB203580 (10 μM), the myosin II ATPase activity inhibitor blebbistatin (50 μM), or the ROCK inhibitor Y27632 (10 μM). *, $P < 0.05$ compared with control α2; §, $P < 0.05$ compared with control α3. (E) Cells were treated at 3.5 h for 30 min with vehicle, DPI (10 μM), SB203580 (10 μM), or both DPI and SB203580. Lysates were prepared and analyzed by SDS-PAGE, followed by immunoblotting with anti-pMLC or anti-MLC antibodies. (F) Cells were treated at 3.5 h for 30 min with vehicle, DPI (10 μM), or SB203580 (10 μM) or incubated for 24 h with the inhibitors shown. Lysates were prepared and analyzed by SDS-PAGE, followed by immunoblotting with anti-α2 or anti-α3 integrin antibodies.

persistence of cell migration directionality. Nox1 inhibition did not affect cell spreading but led to a transient increase in RhoA-dependent cell-matrix contact and to a sustained α2/α3 integrin switch. The loss of directionality observed during cell migration upon Nox1 inhibition was reversed by an α3 integrin blockade, suggesting a major involvement of α3 integrin in this phenotype. These results are consistent with a recent finding showing that epithelial cells from α3 integrin subunit knockout mice migrate with increased persistence (26). Thus, Nox1 would represent a switch between random and directional migration by affecting integrin membrane availability through the RhoA/ROCK/p38 MAPK pathway.

Many reports showed, by using pharmacological inhibition, that ROS produced through an NADPH oxidase-like complex affect cell migration (23, 49). Recent molecular evidence for the involvement of Nox/Duox homologues in the control of cell migration has been reported for Nox2 in endothelial cells (45, 54), Nox1 in vascular smooth muscle cells and colonic epithelial cells (38, 40), Nox4 in myofibroblast and vascular smooth muscle cells (15, 16, 28), and Duox1 in airway epithelial cells (49). In a previous report, we showed that Nox1 controls colonic epithelial cell migration on Col-I by modulating α2 integrin membrane availability. Nox1-dependent ROS production occurred after 4 h of adhesion to Col-I. Nox1 inhibition or downregulation led to a decrease in cell surface and total expression of α2 after 24 h of adhesion to Col-I linked to a loss of directional persistence of migration. In contrast, Nox1 activation by arachidonic acid induced an increase in α2 membrane availability and an increase in the directional persistence of migration. A feature of migration impairment by Nox1

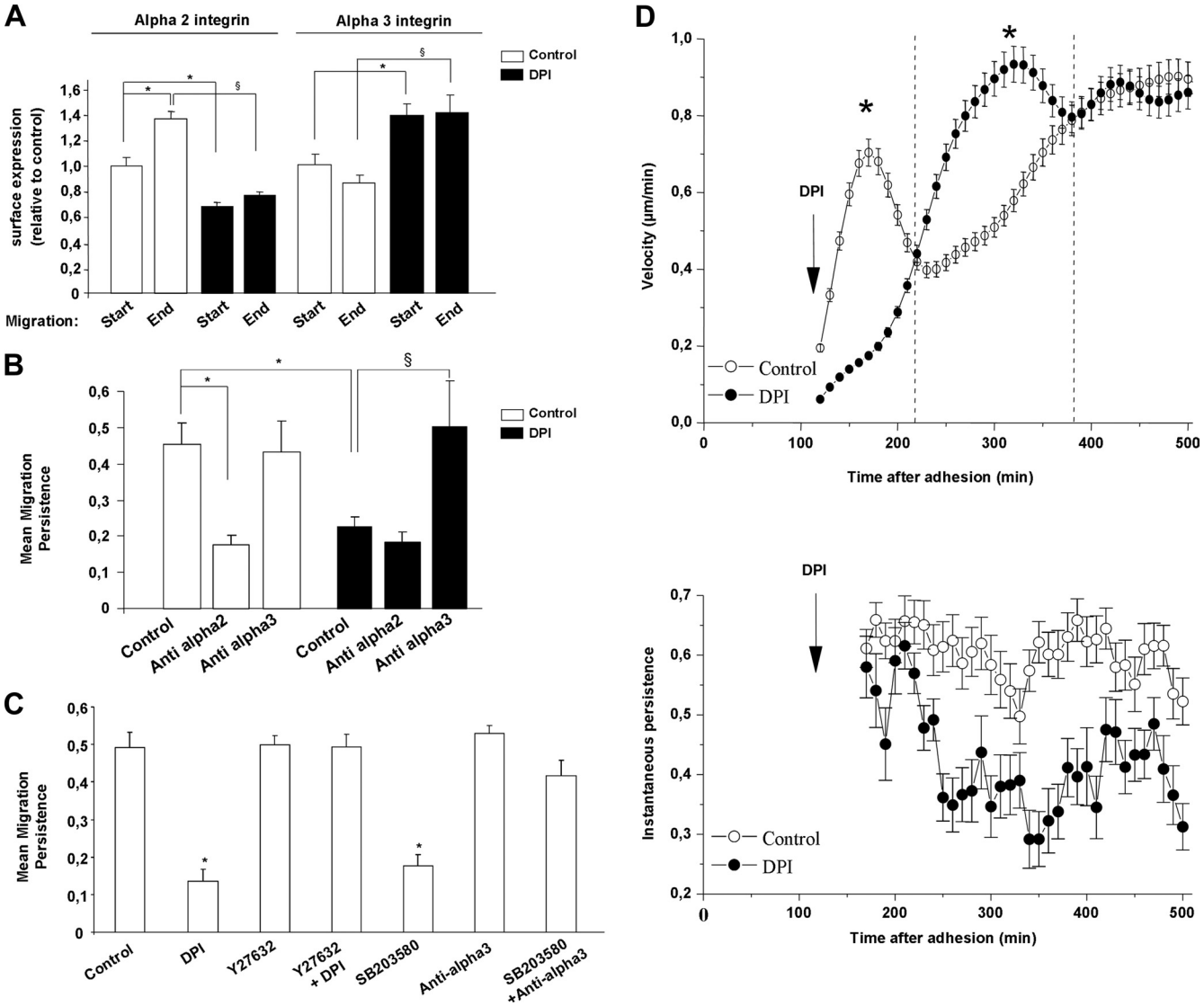

FIG. 6. Nox1-dependent ROS production controls the directionality of cell migration on Col-I by modulation of α2/α3 integrin cell surface expression. A 2D migration experiment was performed on Col-I for 10 h. (A) Cells were seeded onto Col-I and treated with DPI (10 μM) or vehicle after 2 h of adhesion. Cell surface expression of α2 and α3 integrins was assessed by flow cytometry at the start of migration (2 h of adhesion) and at the end of migration (10 h of adhesion). Data are presented as means ± standard errors. * and §, $P < 0.05$ compared with the control. (B) Cells were treated with DPI (10 μM), vehicle, DGEA (α2-blocking peptide; 0.25 mM), or α3-blocking antibodies (10 μg/ml) after 2 h of adhesion to Col-I. Directional persistence was calculated as the ratio of the mean distance to the origin to the mean total migration distance. Data are presented as means ± standard errors. *, $P < 0.05$ compared with the control. (C) Cells were treated after 2 h of adhesion to Col-I with DPI (10 μM), vehicle, α3-blocking antibody (10 μg/ml), SB203580 (10 μM), or Y27632 (10 μM). After 8 h of migration, directional persistence was calculated. Data are presented as means ± standard errors. *, $P < 0.05$ compared with the control. (D) The instantaneous velocity of migration was determined by using the distance measured every 10 min for at least 45 individual cells over 8 h. Instantaneous persistence for each time was calculated as the net translocation observed after six frames divided by the sum of the displacements observed between frames. Instantaneous persistence was calculated for at least 45 individual cells and followed for 8 h. Data are presented as means ± standard errors. *, $P < 0.05$ compared with the control.

downregulation is that neither the total distance nor the mean velocity of migration was affected (38). Thus, impairment of migration by Nox1 could not rely only on the decreased availability of α2 integrin. In this study, we showed that Nox1 affects the RhoA activation state through redox modulation of the activity of p190RhoGAP (Fig. 1). It has been shown by Nimnual et al. that Rac-stimulated ROS production decreases the Rho activation level by increasing the phosphorylation level of p190RhoGAP through inhibition of LMW PTP (31). More recently, Shinohara et al. have shown that Nox1-dependent ROS production inactivates LMW PTP and increases the level of p190RhoGAP activation (41). We show here that Nox1 inhibition induced a transient RhoA overactivation leading to an α2/α3 integrin switch with a decrease in α2 and an increase in α3 integrin cell surface expression while β1 remained constant (Fig. 1 and 2). The transient RhoA overactivation upon

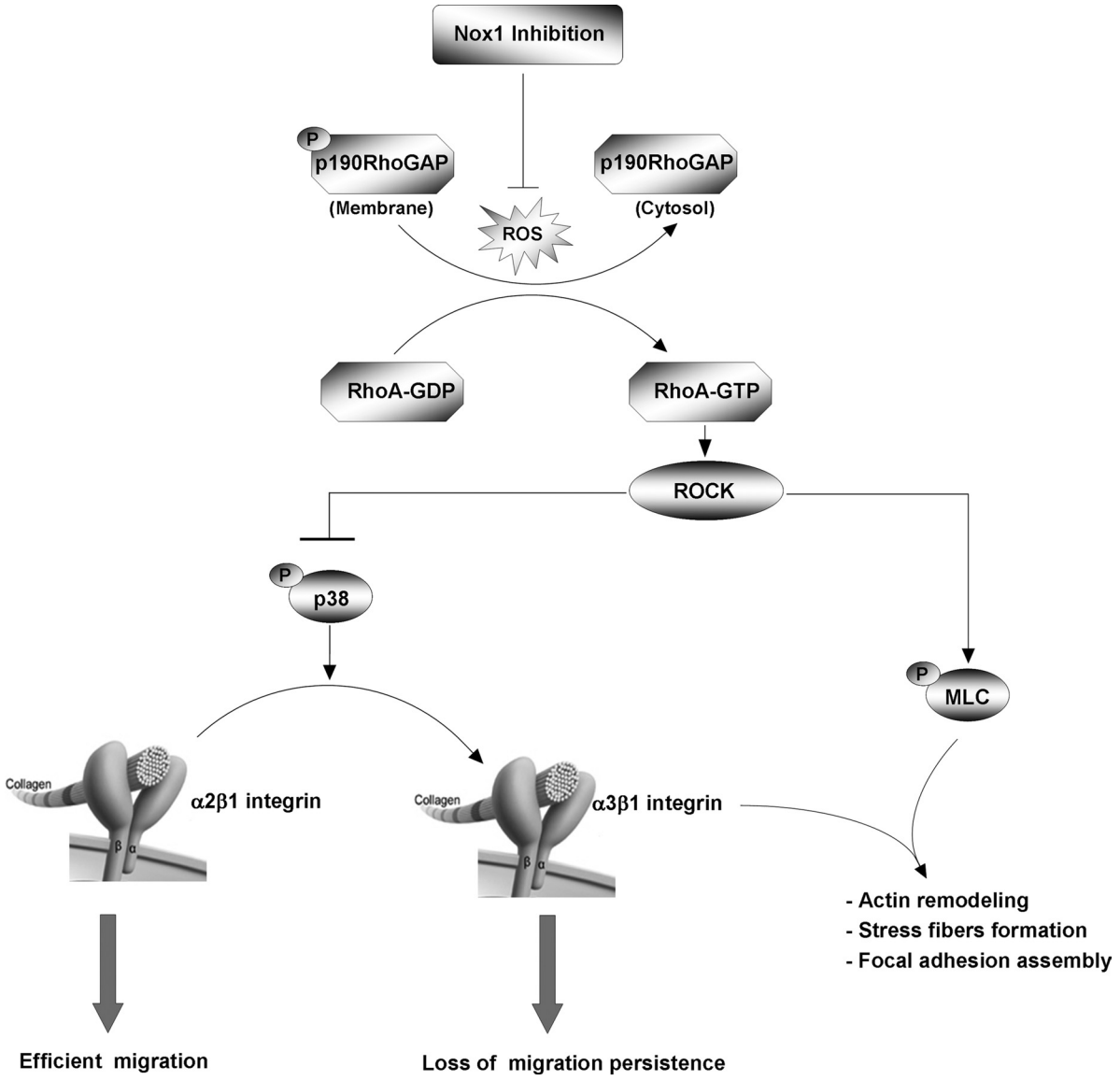

FIG. 7. Schematic depiction of the involvement of Nox1 in α2/α3 integrin switch control and directional migration persistence.

Nox1 inhibition was concomitant with stress fiber formation and focal complex maturation involving α3β1 integrin, which led to a transient reinforcement of cell-matrix contact (Fig. 1 and 4). After the onset of Nox1-dependent ROS production, while RhoA activity returned to normal compared to that of controls, the increase in membrane α3 integrin is sustained, leading to a loss of directional migration (Fig. 6). Previous studies have suggested that high levels of adhesiveness inhibit the speed of cell migration (32) and deadhesion is the rate-limiting step in regulating cell migration under a condition of high cell-substratum adhesiveness. In our experiments, while the mean velocity of migration did not show a significant difference between control and Nox1-inhibited cells, the follow-up of instantaneous velocity showed that the speed of migration was clearly dependent on RhoA and integrin status. A slowdown of velocity was observed during the transient overactivation of RhoA and initiation of the α2/α3 integrin switch by Nox1 inhibition. Then, an increased velocity was observed while RhoA activity returned to normal and the integrin switch was sustained. On the contrary, a sustained decrease in instantaneous persistence was observed under Nox1 inhibition. Since the RhoA activation levels were similar in control and DPI-treated cells after 6 h of adhesion, the cellular persistence of migration does not rely solely on the RhoA activation state. These results suggest that once induced by RhoA activation, the increase in membrane α3 integrin represents a major regulator of cellular migration persistence. These conclusions are supported by recent findings showing that the persistence of migration was increased in keratinocytes from α3 integrin knockout mice. In vitro, these cells compensated for the decrease in α3 integrin by an increase in α6 integrin (26). An integrin switch leading to different motility behavior (directional versus random) has been reported between αvβ3 and α5β1 in fibroblasts (5, 50). These works showed that αvβ3

integrin antagonized α5β1 integrin recycling through outside-in signaling and further affecting the directionality of migration through α5β1 integrin-dependent RhoA activation. On the other hand, it has been shown by Worthylake and Burridge that inhibition of the RhoA/ROCK pathway controls inside-out signaling and modulates integrin activity by promoting remodeling of the actin cytoskeleton and restricting integrin activity and membrane protrusions to the leading edge (53). Our result show that Nox1-dependent ROS production controls cell-matrix contact and the initiation of the integrin switch exclusively through control of the RhoA pathway and that this is mimicked by the $RhoA^{V14}$ mutant (Fig. 4). Nox1 inhibition affects cell migration through RhoA/ROCK pathways by inducing transient cytoskeletal reorganization and by initiating a sustained integrin switch and an increased membrane α3 integrin level. Both cytoskeletal reorganization and α3 integrin sorting after 4 h of adhesion to Col-I led to an increase in cell-matrix closeness and stress fiber formation (Fig. 3). Several RhoA-dependent cytoskeletal rearrangements are regulated by the effector ROCK, which controls the contractility and stabilization of filamentous actin through inactivation of myosin phosphatase and the actin-depolymerizing factor cofilin (2). Cytoskeletal dynamics during cell migration involve complex regulation to mediate the disassembly of F-actin filaments from the rear of the cell and promote lamellipodial assembly at the leading edge (18). The MLC subunit, when phosphorylated, is thought to promote myosin II assembly and increase the actomyosin-based contractility necessary for the generation of stress fibers and the maturation of focal complexes (27). The actin binding protein cofilin binds to F-actin and promotes its severing and depolymerization. When phosphorylated on Ser-3 by the ROCK or PAK upstream LIM kinase, cofilin is unable to bind F-actin (2). Under our experimental conditions, at the onset of Nox1 activation, cofilin phosphorylation was detected whereas MLC was not phosphorylated. Inhibition of Nox1 activation by DPI increased the MLC phosphorylation level but did not further increase cofilin phosphorylation (Fig. 5A). Cofilin phosphorylation detected after 4 h of adhesion suggests that a pathway other than the ROCK pathway controls cofilin phosphorylation in this context. We previously reported that Rac1 is activated after 4 h of adhesion in these cells (7). Such Rac1 activation might be consistent with involvement of the PAK/LIM kinase pathway. Thus, as cofilin was already phosphorylated, Nox1 inhibition and the subsequent RhoA/ROCK activation do not seem to affect the cofilin phosphorylation state. However, we cannot fully exclude the possibility of a local modification of cofilin turnover which could not be detected by a Western blot assay. Finally, the increased MLC phosphorylation state under Nox1 inhibition is consistent with the observed stress fiber formation. As the anti-α3 integrin blocking antibody reversed the formation of stress fibers, we questioned a possible involvement of MLC phosphorylation and cytoskeletal reorganization in the initiation of the integrin switch. MLC phosphorylation induced by DPI or Nox1 knockout was suppressed by Y27632 but unaffected by the anti-α3 integrin blocking antibody (Fig. 5). Inhibition of the actin-myosin II complex by blebbistatin did not block the integrin switch induced by DPI (Fig. 5C). This result confirmed that stress fiber formation associated with MLC phosphorylation is concomitant with initiation of the integrin switch but not involved in its initiation. As the anti-α3 integrin blocking antibody reversed the formation of stress fibers under Nox1 inhibition, α3 integrin should represent a docking site for transient stress fiber formation, leading to the increase in cell-matrix closeness which occurred after 4 h of adhesion. We previously reported that p38 MAPK is involved in the regulation of α2 integrin membrane availability (38). We show here that p38 MAPK phosphorylation was inhibited by DPI and $RhoA^{V14}$ and that that inhibition was reversed by Y27632. Inhibition of p38 MAPK by SB203580 induced the α2/α3 integrin switch but did not affect the phosphorylation level of MLC and the total expression level of the α2 or α3 integrin subunit after 4 and 24 h of adhesion to Col-I. These results were consistent with the involvement of p38 MAPK in the initiation of the integrin switch without any effect on MLC phosphorylation and stress fiber formation. The involvement of p38 MAPK in the recycling of membrane receptors and integrins has been previously described (25, 52, 56). Activated p38 MAPK has been shown to phosphorylate early endosomal antigen 1 and the Rab GDP dissociation inhibitor. In addition, Woods Ignatoski et al. reported a decrease in the surface α4 integrin subunit by Rac1/p38 MAPK activation (52). Overall, these results suggest that the RhoA/ROCK/p38 MAPK pathway affects the recycling of the α2 or α3 integrin, which durably affects the directionality of migration, while the RhoA/ROCK/MLC pathway induces transient cytoskeletal reorganization and increases the strength of adhesion. Thus, in contrast to fibroblasts, where αvβ3 and α5β1 integrin switches lead to different motility behavior by activating the RhoA pathway downstream of the α5β1 integrin (5, 50), in our cell model, the RhoA pathway is an upstream regulator of the α2/α3 integrin switch leading to control of the direction of migration.

We show here that Nox1 controls membrane and total α2 integrin subunit expression levels by two distinct pathways. Indeed, we previously reported that Nox1 knockdown or inhibition decreased the total amount of the α2 integrin subunit after 24 h on Col-I (38). However, Nox1 inhibition or knockout did not affect either the α2 or the α3 integrin total expression level after 4 h of adhesion to Col-I, suggesting that initiation of the membrane α2/α3 integrin switch is not linked to early transcriptional regulation of these integrins (Fig. 4C). This nontranscriptional regulation is also supported by the overexpression of the α2-GFP integrin under the control of the cytomegalovirus promoter (Fig. 2D). In contrast, Nox1 inhibition or knockout induced a decrease in the α2 integrin expression level after 24 h of adhesion to Col-I without affecting the α3 integrin expression level. $RhoA^{V14}$, Y27632, and SB203580 did not modify the α2 or the α3 integrin total expression level after 4 or 24 h of adhesion to Col-I (Fig. 4B and C and 6E). These results suggest that the α2/α3 integrin switch downstream of RhoA/ROCK/p38 MAPK is not linked to the decrease in the total amount of the α2 integrin subunit induced by Nox1 inhibition after 24 h. Thus, Nox1 should control a pathway upstream of RhoA which affects the total expression level of the α2 integrin subunit.

The formation of focal adhesions and closely associated actin stress fibers requires the activation of RhoA (36). The present work shows the major impact of Nox1 as a transient regulator of RhoA on a 2D cell migration model. In three-dimensional (3D) substrata, cells can adopt a persistent mode

of migration with a pseudopod at the leading edge attaching to the ECM, but alternatively, they can move randomly, undergoing amoeboid shape changes (51). Increased RhoA activity has been associated with random migration in 2D and 3D migration models (39). Our present findings suggest that in colon carcinoma cells, Nox1 represents a major regulator of directional persistence of migration by transiently regulating the balance between Rho and Rac. Different reports showed that Rac1 activated Nox1 (reviewed in reference 17), and we have recently shown that Rac1-GTP is needed for Nox1 activation during colonic epithelial cell adhesion to Col-I (6). Fine-tuning of Rac1 and RhoA GTP loading, and certainly the ratio of active Rac1 to RhoA, is needed to maintain cell polarization and the directional persistence of migration. Pankov et al. showed that a low level of active Rac1 is needed to maintain the directional persistence of migration of fibroblasts (33). In this work, we show that an increase in the active RhoA level impairs the directional persistence of migration in favor of random migration. Finally, Nox1 inhibition, leading to the replacement of an integrin efficient for directed migration ($\alpha2\beta1$ integrin) with a nonefficient one ($\alpha3\beta1$ integrin), would represent an amoeboid cell-like phenotype. Recent data showed that blockade of $\alpha2$ integrin limits the occurrence of liver metastases from colon carcinoma cells (46).

The present study provides the first substantial evidence in support of the role of Nox1-dependent ROS in the regulation of integrin turnover during cellular migration. We demonstrated that early Nox1-dependent ROS production controls cellular migration through transient modulation of the RhoA/ROCK pathway and the subsequent regulation of integrin turnover. This involvement of Nox1 in directed migration in cancer cells would represent an interesting target to modulate the efficiency of extravasation during metastasis. Further work is needed to assess the role of Nox1 in amoeboid cell-like migration and in different models of metastasis formation.

ACKNOWLEDGMENTS

Amine Sadok and Laetitia Dahan are recipients of a doctoral fellowship from Association pour la Recherche contre le Cancer. This research was funded by the Institut National de la Santé et de la Recherche Médicale, the Institut National du Cancer, and Cancéropôle PACA, France.

Special thanks go to Leon Espinosa and the imaging platform from the Unité de Recherche sur les Maladies Infectieuses et Tropicales Émergentes (R198) for confocal imaging.

REFERENCES

1. **Abo, A., E. Pick, A. Hall, N. Totty, C. G. Teahan, and A. W. Segal.** 1991. Activation of the NADPH oxidase involves the small GTP-binding protein p21rac1. Nature **353:**668–670.
2. **Amano, M., Y. Fukata, and K. Kaibuchi.** 2000. Regulation and functions of Rho-associated kinase. Exp. Cell Res. **261:**44–51.
3. **Bradley, W. D., S. E. Hernandez, J. Settleman, and A. J. Koleske.** 2006. Integrin signaling through Arg activates p190RhoGAP by promoting its binding to p120RasGAP and recruitment to the membrane. Mol. Biol. Cell **17:**4827–4836.
4. **Chiarugi, P., G. Pani, E. Giannoni, L. Taddei, R. Colavitti, G. Raugei, M. Symons, S. Borrello, T. Galeotti, and G. Ramponi.** 2003. Reactive oxygen species as essential mediators of cell adhesion: the oxidative inhibition of a FAK tyrosine phosphatase is required for cell adhesion. J. Cell Biol. **161:**933–944.
5. **Danen, E. H., J. van Rheenen, W. Franken, S. Huveneers, P. Sonneveld, K. Jalink, and A. Sonnenberg.** 2005. Integrins control motile strategy through a Rho-cofilin pathway. J. Cell Biol. **169:**515–526.
6. **de Carvalho, D. D., A. Sadok, V. Bourgarel-Rey, F. Gattacceca, C. Penel, M. Lehmann, and H. Kovacic.** 2008. Nox1 downstream of 12-lipoxygenase controls cell proliferation but not cell spreading of colon cancer cells. Int. J. Cancer **122:**1757–1764.
7. **del Pozo, M. A., L. S. Price, N. B. Alderson, X. D. Ren, and M. A. Schwartz.** 2000. Adhesion to the extracellular matrix regulates the coupling of the small GTPase Rac to its effector PAK. EMBO J. **19:**2008–2014.
8. **Dunn, G. A., and G. E. Jones.** 2004. Cell motility under the microscope: Vorsprung durch Technik. Nat. Rev. Mol. Cell Biol. **5:**667–672.
9. **Fantini, J., B. Abadie, A. Tirard, L. Remy, J. P. Ripert, A. el Battari, and J. Marvaldi.** 1986. Spontaneous and induced dome formation by two clonal cell populations derived from a human adenocarcinoma cell line, HT29. J. Cell Sci. **83:**235–249.
10. **Friedl, P., and K. Wolf.** 2003. Tumour-cell invasion and migration: diversity and escape mechanisms. Nat. Rev. Cancer **3:**362–374.
11. **Geiszt, M., and T. L. Leto.** 2004. The Nox family of NAD(P)H oxidases: host defense and beyond. J. Biol. Chem. **279:**51715–51718.
12. **Gianni, D., B. Bohl, S. A. Courtneidge, and G. M. Bokoch.** 2008. The involvement of the tyrosine kinase c-Src in the regulation of reactive oxygen species generation mediated by NADPH oxidase-1. Mol. Biol. Cell **19:**2984–2994.
13. **Hall, A.** 2005. Rho GTPases and the control of cell behaviour. Biochem. Soc. Trans. **33:**891–895.
14. **Hanahan, D., and R. A. Weinberg.** 2000. The hallmarks of cancer. Cell **100:**57–70.
15. **Haurani, M. J., M. E. Cifuentes, A. D. Shepard, and P. J. Pagano.** 2008. Nox4 oxidase overexpression specifically decreases endogenous Nox4 mRNA and inhibits angiotensin II-induced adventitial myofibroblast migration. Hypertension **52:**143–149.
16. **Hilenski, L. L., R. E. Clempus, M. T. Quinn, J. D. Lambeth, and K. K. Griendling.** 2004. Distinct subcellular localizations of Nox1 and Nox4 in vascular smooth muscle cells. Arterioscler. Thromb. Vasc. Biol. **24:**677–683.
17. **Hordijk, P. L.** 2006. Regulation of NADPH oxidases: the role of Rac proteins. Circ. Res. **98:**453–462.
18. **Huang, T. Y., C. DerMardirossian, and G. M. Bokoch.** 2006. Cofilin phosphatases and regulation of actin dynamics. Curr. Opin. Cell Biol. **18:**26–31.
19. **Knaus, U. G., P. G. Heyworth, T. Evans, J. T. Curnutte, and G. M. Bokoch.** 1991. Regulation of phagocyte oxygen radical production by the GTP-binding protein Rac 2. Science **254:**1512–1515.
20. **Kwon, J., S. R. Lee, K. S. Yang, Y. Ahn, Y. J. Kim, E. R. Stadtman, and S. G. Rhee.** 2004. Reversible oxidation and inactivation of the tumor suppressor PTEN in cells stimulated with peptide growth factors. Proc. Natl. Acad. Sci. USA **101:**16419–16424.
21. **Lambeth, J. D.** 2004. NOX enzymes and the biology of reactive oxygen. Nat. Rev. Immunol. **4:**181–189.
22. **Li, Q., Y. Zhang, J. J. Marden, B. Banfi, and J. F. Engelhardt.** 2008. Endosomal NADPH oxidase regulates c-Src activation following hypoxia/reoxygenation injury. Biochem. J. **411:**531–541.
23. **Liu, R., B. Li, and M. Qiu.** 2001. Elevated superoxide production by active H-ras enhances human lung WI-38VA-13 cell proliferation, migration and resistance to TNF-α. Oncogene **20:**1486–1496.
24. **Llobet, A., V. Beaumont, and L. Lagnado.** 2003. Real-time measurement of exocytosis and endocytosis using interference of light. Neuron **40:**1075–1086.
25. **Macé, G., M. Miaczynska, M. Zerial, and A. R. Nebreda.** 2005. Phosphorylation of EEA1 by p38 MAP kinase regulates mu opioid receptor endocytosis. EMBO J. **24:**3235–3246.
26. **Margadant, C., K. Raymond, M. Kreft, N. Sachs, H. Janssen, and A. Sonnenberg.** 2009. Integrin $\alpha3\beta1$ inhibits directional migration and wound re-epithelialization in the skin. J. Cell Sci. **122:**278–288.
27. **Matsumura, F.** 2005. Regulation of myosin II during cytokinesis in higher eukaryotes. Trends Cell Biol. **15:**371–377.
28. **Meng, D., D.-D. Lv, and J. Fang.** 2008. Insulin-like growth factor-I induces reactive oxygen species production and cell migration through Nox4 and Rac1 in vascular smooth muscle cells. Cardiovasc. Res. **80:**299–308.
29. **Moissoglu, K., and M. A. Schwartz.** 2006. Integrin signalling in directed cell migration. Biol. Cell **98:**547–555.
30. **Moldovan, L., N. I. Moldovan, R. H. Sohn, S. A. Parikh, and P. J. Goldschmidt-Clermont.** 2000. Redox changes of cultured endothelial cells and actin dynamics. Circ. Res. **86:**549–557.
31. **Nimnual, A. S., L. J. Taylor, and D. Bar-Sagi.** 2003. Redox-dependent downregulation of Rho by Rac. Nat. Cell Biol. **5:**236–241.
32. **Palecek, S. P., J. C. Loftus, M. H. Ginsberg, D. A. Lauffenburger, and A. F. Horwitz.** 1997. Integrin-ligand binding properties govern cell migration speed through cell-substratum adhesiveness. Nature **385:**537–540.
33. **Pankov, R., Y. Endo, S. Even-Ram, M. Araki, K. Clark, E. Cukierman, K. Matsumoto, and K. M. Yamada.** 2005. A Rac switch regulates random versus directionally persistent cell migration. J. Cell Biol. **170:**793–802.
34. **Pegtel, D. M., S. I. Ellenbroek, A. E. Mertens, R. A. van der Kammen, J. de Rooij, and J. G. Collard.** 2007. The Par-Tiam1 complex controls persistent migration by stabilizing microtubule-dependent front-rear polarity. Curr. Biol. **17:**1623–1634.
35. **Pellinen, T., A. Arjonen, K. Vuoriluoto, K. Kallio, J. A. Fransen, and J. Ivaska.** 2006. Small GTPase Rab21 regulates cell adhesion and controls endosomal traffic of β1-integrins. J. Cell Biol. **173:**767–780.

36. **Ridley, A. J., and A. Hall.** 1992. The small GTP-binding protein rho regulates the assembly of focal adhesions and actin stress fibers in response to growth factors. Cell **70:**389–399.
37. **Ridley, A. J., M. A. Schwartz, K. Burridge, R. A. Firtel, M. H. Ginsberg, G. Borisy, J. T. Parsons, and A. R. Horwitz.** 2003. Cell migration: integrating signals from front to back. Science **302:**1704–1709.
38. **Sadok, A., V. Bourgarel-Rey, F. Gattacceca, C. Penel, M. Lehmann, and H. Kovacic.** 2008. Nox1-dependent superoxide production controls colon adenocarcinoma cell migration. Biochim. Biophys. Acta **1783:**23–33.
39. **Sahai, E., and C. J. Marshall.** 2003. Differing modes of tumour cell invasion have distinct requirements for Rho/ROCK signalling and extracellular proteolysis. Nat. Cell Biol. **5:**711–719.
40. **Schröder, K., I. Helmcke, K. Palfi, K. H. Krause, R. Busse, and R. P. Brandes.** 2007. Nox1 mediates basic fibroblast growth factor-induced migration of vascular smooth muscle cells. Arterioscler. Thromb. Vasc. Biol. **27:** 1736–1743.
41. **Shinohara, M., W. H. Shang, M. Kubodera, S. Harada, J. Mitsushita, M. Kato, H. Miyazaki, H. Sumimoto, and T. Kamata.** 2007. Nox1 redox signaling mediates oncogenic Ras-induced disruption of stress fibers and focal adhesions by down-regulating Rho. J. Biol. Chem. **282:**17640–17648.
42. **Suh, Y. A., R. S. Arnold, B. Lassegue, J. Shi, X. Xu, D. Sorescu, A. B. Chung, K. K. Griendling, and J. D. Lambeth.** 1999. Cell transformation by the superoxide-generating oxidase Mox1. Nature **401:**79–82.
43. **Terada, L. S.** 2006. Specificity in reactive oxidant signaling: think globally, act locally. J. Cell Biol. **174:**615–623.
44. **Ushio-Fukai, M.** 2006. Localizing NADPH oxidase-derived ROS. Sci. STKE **2006:**re8.
45. **Ushio-Fukai, M., and R. W. Alexander.** 2004. Reactive oxygen species as mediators of angiogenesis signaling: role of NAD(P)H oxidase. Mol. Cell. Biochem. **264:**85–97.
46. **van der Bij, G. J., S. J. Oosterling, M. Bogels, F. Bhoelan, D. M. Fluitsma, R. H. Beelen, S. Meijer, and M. van Egmond.** 2008. Blocking α2 integrins on rat CC531s colon carcinoma cells prevents operation-induced augmentation of liver metastases outgrowth. Hepatology **47:**532–543.
47. **van der Flier, A., and A. Sonnenberg.** 2001. Function and interactions of integrins. Cell Tissue Res. **305:**285–298.
48. **Verschueren, H.** 1985. Interference reflection microscopy in cell biology: methodology and applications. J. Cell Sci. **75:**279–301.
49. **Wesley, U. V., P. F. Bove, M. Hristova, S. McCarthy, and A. van der Vliet.** 2007. Airway epithelial cell migration and wound repair by ATP-mediated activation of dual oxidase 1. J. Biol. Chem. **282:**3213–3220.
50. **White, D. P., P. T. Caswell, and J. C. Norman.** 2007. αvβ3 and α5β1 integrin recycling pathways dictate downstream Rho kinase signaling to regulate persistent cell migration. J. Cell Biol. **177:**515–525.
51. **Wolf, K., I. Mazo, H. Leung, K. Engelke, U. H. von Andrian, E. I. Deryugina, A. Y. Strongin, E. B. Brocker, and P. Friedl.** 2003. Compensation mechanism in tumor cell migration: mesenchymal-amoeboid transition after blocking of pericellular proteolysis. J. Cell Biol. **160:**267–277.
52. **Woods Ignatoski, K. M., N. K. Grewal, S. Markwart, D. L. Livant, and S. P. Ethier.** 2003. p38MAPK induces cell surface α4 integrin downregulation to facilitate erbB-2-mediated invasion. Neoplasia **5:**128–134.
53. **Worthylake, R. A., and K. Burridge.** 2003. RhoA and ROCK promote migration by limiting membrane protrusions. J. Biol. Chem. **278:**13578–13584.
54. **Wu, R. F., Y. C. Xu, Z. Ma, F. E. Nwariaku, G. A. Sarosi, Jr., and L. S. Terada.** 2005. Subcellular targeting of oxidants during endothelial cell migration. J. Cell Biol. **171:**893–904.
55. **Yamaguchi, H., J. Wyckoff, and J. Condeelis.** 2005. Cell migration in tumors. Curr. Opin. Cell Biol. **17:**559–564.
56. **Zwang, Y., and Y. Yarden.** 2006. p38 MAP kinase mediates stress-induced internalization of EGFR: implications for cancer chemotherapy. EMBO J. **25:**4195–4206.